Article

Humanized and Defucosylated Antibody against Podoplanin (humLpMab-23-f) Exerted Antitumor Activities in Human Tumor Xenograft Models

Hiroyuki Suzuki [1,2,*,†], Tomokazu Ohishi [3,4,†], Mika K. Kaneko [1,2] and Yukinari Kato [1,2,*]

[1] Department of Molecular Pharmacology, Tohoku University Graduate School of Medicine, 2-1 Seiryo-machi, Aoba-ku, Sendai 980-8575, Miyagi, Japan; k.mika@med.tohoku.ac.jp (M.K.K.)
[2] Department of Antibody Drug Development, Tohoku University Graduate School of Medicine, 2-1 Seiryo-machi, Aoba-ku, Sendai 980-8575, Miyagi, Japan
[3] Institute of Microbial Chemistry (BIKAKEN), Numazu, Microbial Chemistry Research Foundation, 18-24 Miyamoto, Numazu-shi 410-0301, Japan; ohishit@bikaken.or.jp (T.O.)
[4] Institute of Microbial Chemistry (BIKAKEN), Laboratory of Oncology, Microbial Chemistry Research Foundation, 3-14-23 Kamiosaki, Shinagawa-ku 141-0021, Tokyo, Japan
* Correspondence: hiroyuki.suzuki.b4@tohoku.ac.jp (H. S.); yukinari.kato.e6@tohoku.ac.jp (Y.K.); Tel.: +81-22-717-8207 (H.S., Y.K.).
† Contributed equally to this work.

Simple Summary: Podoplanin (PDPN) is a mucin-like transmembrane glycoprotein that plays essential roles in tumor progression. PDPN-expressing tumors exhibit an aggressive phenotype including increased invasiveness, epithelial-to-mesenchymal transition, and stemness which are critical for the tumor malignant progression. Furthermore, PDPN-positive cancer-associated fibroblasts mediate an immunosuppressive tumor microenvironment which reduces antitumor immunity. Therefore, monoclonal antibodies (mAbs) against PDPN have been evaluated in preclinical models. In this study, we developed a humanized and defucosylated mAb against PDPN (humLpMab-23-f) and evaluated it for its antibody-dependent cellular cytotoxicity (ADCC) and antitumor effect in xenograft models of human tumor cells. The humLpMab-23-f exerted antitumor activities against PDPN-overexpressed CHO-K1 and endogenous PDPN-positive PC-10 and LN319 xenograft-inoculated mice.

Abstract: We previously developed a highly sensitive and specific anti-PDPN mAb, LpMab-23 (mouse IgG_1, kappa). In this study, we produced a humanized IgG_1 version (humLpMab-23) and its defucosylated form (humLpMab-23-f) of an anti-PDPN mAb to potentiate the ADCC activity. The humLpMab-23 could recognize PDPN-overexpressed Chinese hamster ovary (CHO)-K1 (CHO/PDPN) and PDPN-positive PC-10 and LN319 cells by flow cytometry. Furthermore, we found that humLpMab-23-f exerted ADCC and complement-dependent cytotoxicity against CHO/PDPN, PC-10 and LN319 cells *in vitro* and exhibited potent antitumor activities in the xenograft models. These results indicated that humLpMab-23-f could be useful for an antibody treatment regimen for PDPN-positive human cancers.

Keywords: PDPN; lung cancer; glioblastoma; monoclonal antibody; antitumor activities; mouse xenograft model; antibody-dependent cellular cytotoxicity

1. Introduction

PDPN is a type I transmembrane glycoprotein and has an extracellular domain, a transmembrane domain, and a short cytoplasmic tail. The PDPN extracellular domain possesses platelet aggregation-stimulating (PLAG)1 to PLAG3 domains [1]. Furthermore, several PLAG-like domains (PLDs) were identified, and one of PLDs is called as the PLAG4 domain [1]. PDPN is modified with mucin *O*-glycans with galactose-linked β1, 3 to *N*-acetyl-galactosamine (GalNAc) [2,3]. The *O*-glycosylated PLAG3 at Thr52 or PLD/PLAG4 have been reported to interact with a platelet receptor, C-type lectin-like receptor 2 (CLEC-2), which is important for PDPN-induced

 doi:10.20944/preprints202308.1756.v1

platelet aggregation [3,4]. The PDPN intracellular domain can recruit ezrin, radixin, and moesin (ERM) complex that regulates actin cytoskeleton reorganization and epithelial to mesenchymal transition (EMT) [5,6]. Furthermore, PDPN interacts with matrix metalloproteinases [7] and hyaluronan receptor CD44 [8,9]. The complex was formed in tumor invadopodia, which promotes the hyaluronan-binding and extracellular matrix (ECM) degradation [8,9]. Furthermore, PDPN mediates the diverse pattern of tumor invasion including collective invasion in squamous cell carcinomas [10] and ameboid invasion in melanoma [11].

Overexpression of PDPN has been reported in many tumors, including squamous cell carcinomas in head and neck [12], oral [13], and esophagus [14], malignant gliomas [15,16], and mesotheliomas [17]. The overexpression of PDPN is associated with poor clinical outcomes [1]. Furthermore, PDPN is also expressed in cancer-associated fibroblasts (CAFs), a major component of the tumor microenvironment (TME). CAFs are reported to enhance cancer cell survival and affect therapeutic outcome. CAFs are also involved in the formation of immunosuppressive TME which could reduce the antitumor immunity [18]. Elevated PDPN staining in CAFs is correlated with poor prognosis in lung [19-21], breast [22], and pancreatic [23] cancer patients. Therefore, PDPN has been considered as a useful diagnostic marker and an attractive therapeutic target for tumors.

Our groups previously established several mAbs against human PDPN. A clone NZ-1 recognizes between PLAG2 and PLAG3 domain of PDPN, possesses a neutralizing activity for CLEC-2 binding, and inhibits the platelet aggregation and hematogenous pulmonary metastasis [24]. NZ-8 (a rat-human chimeric antibody derived from NZ-1) exhibited ADCC activities and antitumor effects against malignant pleural mesothelioma in the presence of human natural killer (NK) cells [17]. A mouse-human chimeric anti-PDPN mAb, chLpMab-7 recognizes a PLD domain. chLpMab-7 never showed the neutralization activity through inhibition of PDPN–CLEC-2 interaction but suppressed tumor growth and hematogenous pulmonary metastasis [25]. These findings indicated that ADCC and CDC activities are critical in targeting PDPN-positive tumors.

We also developed a cancer-specific monoclonal antibody (CasMab) method that uses flow cytometry and immunohistochemistry to select mAbs that exhibited reactivity with cancer cells but reduced reactivity with normal cells [26]. LpMab-2 is a CasMab, which recognizes the glycopeptide structure from Thr55 to Leu64 of PDPN [26]. LpMab-23, another CasMab against PDPN, recognizes a peptide structure from Gly54 to Leu64 of PDPN [27]. These PDPN-targeting CasMabs [26-28] have been applied to chimeric antigen receptor (CAR)-T therapy in mice preclinical models [29-31].

The ADCC activity is mediated by NK cells through binding of the FcγRIIIa to mAbs Fc region. A core fucose deficiency on the *N*-glycan in the Fc region facilitates the binding of Fc to FcγRIIIa on effector cells [32]. In recombinant mAb production in Chinese hamster ovary (CHO) cells, Fucosyltransferases 8 (Fut8)-deficient CHO is ideal host to produce completely defucosylated mAbs for therapeutic use [33]. We produced mouse-human chimeric and defucosylated forms of anti-PDPN mAbs from LpMab-2 and LpMab-23, which showed the antitumor effect in mouse xenograft model.

In this study, we produced a humanized and defucosylated anti-PDPN mAb (humLpMab-23-f), and evaluated the ability to induce ADCC and CDC or antitumor efficacy against PDPN-positive tumor cells.

2. Materials and Methods

2.1. Cell lines

CHO-K1 was obtained from the American Type Culture Collection (ATCC, Manassas, VA, USA). CHO/PDPN was established as described previously [26]. PC-10 was purchased from Immuno-Biological Laboratories Co., Ltd. (Gunma, Japan). CHO-K1, CHO/PDPN, and PC-10 were cultured in Roswell Park Memorial Institute（RPMI）-1640 medium [Nacalai Tesque, Inc. (Nacalai), Kyoto, Japan]. LN319 was purchased from Addexbio Technologies (San Diego, CA, USA) and cultured in Dulbecco's modified Eagle's medium (DMEM) medium (Nacalai). Both media were supplemented with 10% heat-inactivated fetal bovine serum [FBS, Thermo Fisher Scientific, Inc. (Thermo), Waltham, MA], 100 units/ml of penicillin, 100 μg/ml streptomycin, and 0.25 μg/ml

 doi:10.20944/preprints202308.1756.v1

amphotericin B (Nacalai). ExpiCHO-S and Fut8-deficient ExpiCHO-S (BINDS-09) were cultured following manufacturer's instructions. All cell lines were cultured at 37°C in a humidified atmosphere with 5% CO_2 and 95% air.

2.2. Recombinant mAb production

For the generation of a humanized anti-human PDPN mAb (humLpMab-23), the complementarity determining region (CDR) of LpMab-23 V_H, frame sequences of V_H in human Ig, and C_H of human IgG_1 were cloned into the pCAG-Neo vector [FUJIFILM Wako Pure Chemical Corporation (Wako), Osaka, Japan]. The CDR of LpMab-23 V_L, frame sequences of V_L in human Ig, and C_L of human lambda chain were cloned into the pCAG-Ble vector (Wako). The antibody expression vectors of humLpMab-23 were transfected into ExpiCHO-S or BINDS-09 using the ExpiCHO-S Expression System (Thermo Fisher Scientific, Inc.). Produced mAbs were named as humLpMab-23 and humLpMab-23-f, respectively. humLpMab-23 and humLpMab-23-f were purified using Ab-Capcher (ProteNova Co., Ltd., Kagawa, Japan). Human IgG was purchased from Sigma-Aldrich Corp. (St. Louis, MO).

2.3. Animal Experiments for mice xenograft model

All animal experiments for antitumor activity by humLpMab-23-f were approved (approval no. 2020-035) by the Institutional Committee for Experiments of the Institute of Microbial Chemistry (Numazu, Japan). Mice were monitored and maintained as described previously [34].

2.4. Flow cytometry

CHO-K1, CHO/PDPN, PC-10, and LN319 cells were collected using 0.25% trypsin and 1 mM ethylenediamine tetraacetic acid (EDTA; Nacalai). The cells (1×10^5 cells/sample) were treated with humLpMab-23 or blocking buffer (control) (0.1% BSA in PBS) for 30 min at 4°C. Next, the cells were treated with Fluorescein isothiocyanate (FITC)-conjugated anti-human IgG (1:2,000; Sigma-Aldrich Corp., St. Louis, MO) for 30 min at 4°C. The EC 800 Cell Analyzer (Sony Corp., Tokyo, Japan) was used to collect the fluorescence data, which were analyzed using FlowJo [BD Biosciences (BD), Franklin Lakes, NJ, USA].

2.5. Determination of the binding affinity by flow cytometry

After being suspended in 100 μL of serially diluted humLpMab-23, the cells were then incubated with 1:200 of FITC-conjugated anti-human IgG. The EC800 Cell Analyzer was then used to gather fluorescence data. The binding isotherms were fitted into the built-in, one-site binding model in GraphPad PRISM 8 (GraphPad Software, Inc., La Jolla, CA) to calculate the dissociation constant (K_D).

2.6. ADCC

Human NK cells were purchased from Takara Bio, Inc., (Shiga, Japan). Target cells were labeled with 10 μg/mL Calcein AM (Thermo Fisher Scientific, Inc.) and resuspended in the same medium. Target cells were plated in 96-well plates (1×10^4 cells/well) and mixed with the human NK cells, humLpMab-23-f, or control human IgG. After a 4.5-hour incubation, Calcein AM release to the supernatant from each well was measured. Fluorescence intensity was determined using a microplate reader (Power Scan HT; BioTek Instruments, Winooski, VT) with excitation and emission wavelengths of 485 and 538 nm, respectively. Cytotoxicity (% of lysis) was calculated as % lysis = (E - S)/(M - S) × 100, where E is the fluorescence of combined target and effector cells, S is spontaneous fluorescence of target cells only, and M is maximum fluorescence measured after lysing all cells with a buffer containing 0.5% Triton X-100, 10 mM Tris-HCl (pH 7.4), and 10 mM of EDTA.

2.7. CDC

 doi:10.20944/preprints202308.1756.v1

The Calcein AM-labeled target cells were plated and mixed with anti-PDPN antibodies and rabbit complement (final dilution 1:10, Low-Tox-M Rabbit Complement; Cedarlane Laboratories, Hornby, ON, Canada) and 100 μg/ml of control human IgG or humLpMab-23-f. Following incubation for 4.5 h at 37°C, the Calcein release into the medium was measured, as described above.

2.8. Antitumor activity of humLpMab-23-f in xenografts of CHO-K1, CHO/PDPN, PC-10, and LN319 cells.

CHO-K1, CHO/PDPN, PC-10, and LN319 cells (0.3 mL of 1.33 × 10^8 cells/mL in DMEM) were mixed with 0.5 mL of BD Matrigel Matrix Growth Factor Reduced (BD Biosciences, San Jose, CA). BALB/c nude mice (Charles River Laboratories, Inc) were injected subcutaneously in the left flank (100 μL) with the suspension mentioned earlier (5 × 10^6 cells). After day 6, 100 μg of humLpMab-23-f (n=8) and control human IgG (n=8) in 100 μL PBS were injected into mice through intraperitoneal injection (i.p.). Additional antibodies were injected on days 14 and 21. Human NK cells (8.0 × 10^5 cells) were injected around the tumors on days 6, 14, and 21. The tumor volume was measured on days 6, 11, 14, 18, 21, and 25 after the inoculation of cells. Twenty-five days after cell inoculation, all mice were euthanized by cervical dislocation and tumor diameters and volumes were determined as previously described.

2.9. Statistical analyses

All data are shown as mean ± standard error of the mean (SEM). In ADCC, CDC, and tumor weight, Welch's *t*-test was used for the statistical analyses. In tumor volume and mouse weight, ANOVA with Sidak's post hoc test was used. $P<0.05$ was considered to indicate a statistically significant difference.

3. Results

3.1. Production of humanized anti-PDPN mAb, humLpMab-23

We previously established an anti-PDPN mAb (LpMab-23; mouse IgG_1, kappa) by the immunization of PDPN ectodomain produced by glioblastoma LN229 cells [35]. LpMab-23 was shown to be useful for flow cytometry [35] and immunohistochemistry [36]. In this study, we engineered a humanized LpMab-23 (humLpMab-23) by fusing the V_H and V_L CDRs of LpMab-23 with the C_H and C_L chains of human IgG_1, respectively (Figure 1A). The humLpMab-23 detected CHO/PDPN cells, but not parental CHO-K1 cells (Figure 1B). Furthermore, humLpMab-23 reacted PDPN-positive glioblastoma LN319 and lung squamous cell carcinoma PC-10 cells (Figure 1C).

A kinetic analysis of the interactions of humLpMab-23 with CHO/PDPN, LN319, and PC-10 was performed by flow cytometry. As shown in Figure. 1D, the K_D for the interaction of humLpMab-23 with CHO/PDPN, LN319, and PC-10 were 4.7 × 10^{-9} M, 4.9 × 10^{-9} M, and 5.4 × 10^{-9} M, respectively. These results suggest that humLpMab-23-f demonstrates a high affinity for PDPN-positive cells.

Preprints (www.preprints.org) | NOT PEER-REVIEWED | Posted: 24 August 2023 doi:10.20944/preprints202308.1756.v1

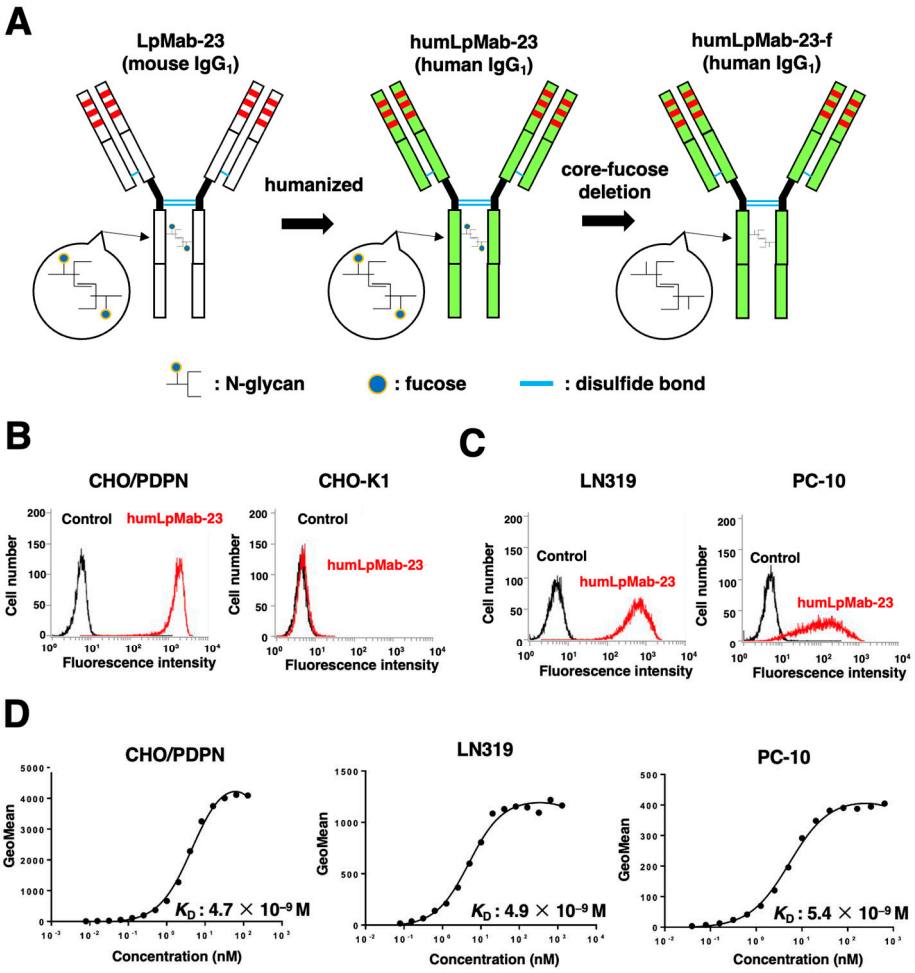

Figure 1. Flow cytometry using humLpMab-23. (**A**) A humanized IgG1 mAb, humLpMab-23 was generated from LpMab-23-f (mouse IgG1). The core-fucose-deficient form (humLpMab-23-f) was produced using Fut8-deficient ExpiCHO-S (BINDS-09) cells. (**B**) CHO-K1 and CHO/PDPN cells were treated with 1 μg/ml of humLpMab-23 or buffer control, followed by FITC-conjugated anti-human IgG. (**C**) LN319 and PC-10 cells were treated with 1 μg/ml of humLpMab-23 or buffer control, followed by Alexa Fluor 488-conjugated anti-human IgG. (**D**) Determination of the binding affinity of humLpMab-23 using flow cytometry. CHO/PDPN, LN319 and PC-10 cells were suspended in humLpMab-23 at indicated concentrations, followed by the addition of FITC-conjugated anti-human IgG. Fluorescence data were analyzed using the EC800 Cell Analyzer. The dissociation constant (K_D) was calculated by GraphPad Prism 8.

3.2. ADCC and CDC by humLpMab-23-f against CHO/PDPN cells.

We next produced humLpMab-23-f, the core-fucose deleted version of humLpMab-23 using Fut8-deficient ExpiCHO-S (BINDS-09) cells (Figure 1A) and examined whether humLpMab-23-f could exert ADCC against CHO/PDPN cells in the presence of human NK-cells. The humLpMab-23-f showed ADCC (51.6% cytotoxicity) against CHO/PDPN cells more effectively than the control human IgG (13.6% cytotoxicity; $P<0.05$) (Figure 2A). There was no difference between humLpMab-23-f and control human IgG in ADCC against CHO-K1 (Figure 2B).

We then investigated whether humLpMab-23-f could show CDC against CHO/PDPN cells. As shown in Figure 2C, humLpMab-23-f could exert CDC (69.2% cytotoxicity) in CHO/PDPN cells compared with that elicited by control human IgG (15.0% cytotoxicity; $P<0.05$). There was no difference between humLpMab-23-f and control human IgG in CDC against CHO-K1 (Figure 2D). These results indicated that humLpMab-23-f possessed potent ADCC and CDC activities against CHO/PDPN cells.

Preprints (www.preprints.org) | NOT PEER-REVIEWED | Posted: 24 August 2023 doi:10.20944/preprints202308.1756.v1

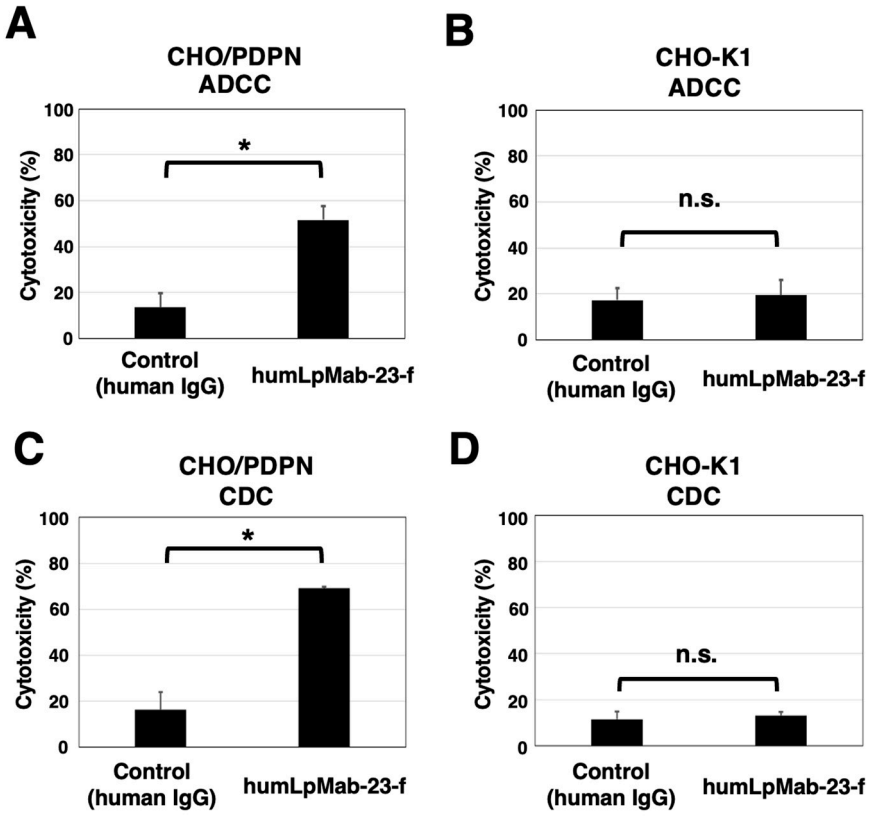

Figure 2. The ADCC and CDC activities mediated by humLpMab-23-f in CHO-K1 and CHO/PDPN cells. (**A**,**C**) The ADCC induced by humLpMab-23-f or control human IgG against CHO/PDPN (**A**) and CHO-K1 (**C**) cells. (**B**,**D**) The CDC induced by humLpMab-23-f or control human IgG against CHO/PDPN (**B**) and CHO-K1 (**D**) cells. Values are shown as mean ± SEM. Asterisks indicate statistical significance (*P< 0.05; Welch's *t*-test). n.s., not significant. ADCC, antibody-dependent cellular cytotoxicity; CDC, complement-dependent cytotoxicity.

3.3. Antitumor effects of humLpMab-23-f against CHO/PDPN xenograft.

Following the inoculation of CHO/PDPN in BALB/c nude mice, humLpMab-23-f and control human IgG were intraperitoneally injected into the mice on days 6, 14, and 21. Furthermore, human NK cells were injected around the tumors on days 6, 14, and 21. On days 6, 11, 14, 18, 21, and 25 after the inoculation of CHO/PDPN, the tumor volume was measured. The humLpMab-23-f administration resulted in a significant reduction of tumors on days 18 (P<0.01), 21 (P<0.01), and 25 (P<0.01) compared with that of human IgG (Figure 3A). The humLpMab-23-f administration resulted in about 73% reduction of the volume compared with that of the control human IgG on day 25 post-injection. The weight of CHO/PDPN tumors treated with humLpMab-23-f was significantly lower than that treated with control human IgG (90% reduction; P<0.01; Figure 3C). CHO/PDPN tumors that were resected from mice on day 25 are demonstrated in Figure 3E. The body weight was not affected in CHO/PDPN tumor-bearing mice treated with humLpMab-23-f and control human IgG (Figure 3G).

In the CHO-K1-bearing mice, humLpMab-23-f and control human IgG were injected intraperitoneally into mice on days 6, 14, and 21 after the inoculation. Furthermore, human NK cells were injected around the tumors. No difference was observed between humLpMab-23-f and control human IgG in CHO-K1 xenograft volume (Figure 3B) and weight (Figure 3D). CHO-K1 tumors that were resected from mice on day 25 are shown in Figure 3F. The body weight loss was not observed (Figure 3H). Supplementary Figure S1 showed the body appearance in CHO/PDPN and CHO-K1 xenografts-inoculated mice treated with human IgG and humLpMab-23-f on day 25.

Preprints (www.preprints.org) | NOT PEER-REVIEWED | Posted: 24 August 2023 doi:10.20944/preprints202308.1756.v1

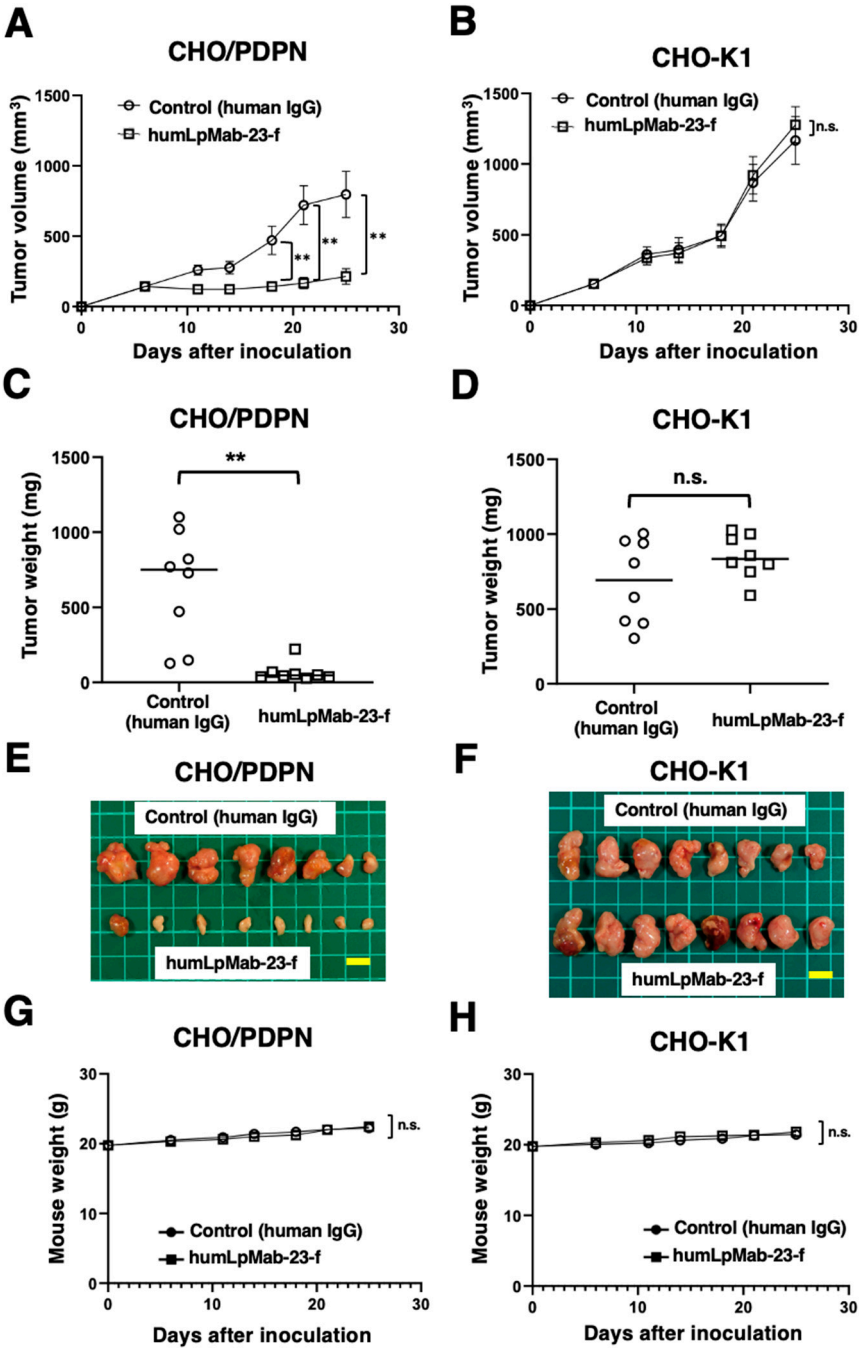

Figure 3. Antitumor activity of humLpMab-23-f against CHO-K1 and CHO/PDPN xenograft. (**A**,**B**) CHO/PDPN (**A**) and CHO-K1 (**B**) cells were subcutaneously injected into BALB/c nude mice (day 0). On day 6, 100 μg of humLpMab-23-f or control human IgG was injected intraperitoneally into mice. Additional antibodies were injected on days 14 and 21. The human NK cells were also injected around the tumors on days 6, 14, and 21. The tumor volume was measured on days 6, 11, 14, 18, 21, and 25. Values are presented as the mean ± SEM. **P<0.01 (ANOVA and Sidak's multiple comparisons test). (**C**,**D**) Tumor weight of CHO/PDPN (**C**) and CHO-K1 (**D**) xenograft tumors on day 25. Values are presented as the mean ± SEM. **P<0.01 (Welch's *t*-test). (**E**,**F**) The CHO/PDPN (**E**) and CHO-K1 (**F**) xenograft tumors on day 25 (scale bar, 1 cm). (**G**,**H**) The body weight of CHO/PDPN (**G**) and CHO-K1 (**H**) xenograft-bearing mice treated with control human IgG and humLpMab-23-f. n.s., not significant.

3.4. ADCC and CDC by humLpMab-23-f against LN319 and PC-10 cells.

Preprints (www.preprints.org) | NOT PEER-REVIEWED | Posted: 24 August 2023 doi:10.20944/preprints202308.1756.v1

We next investigated the ADCC of humLpMab-23-f against endogenous PDPN-positive LN319 and PC-10 cells. As shown in Figure 4A, humLpMab-23-f showed ADCC (47.7% cytotoxicity) against LN319 cells more potently than did the control human IgG (15.8% cytotoxicity; P<0.01). Furthermore, humLpMab-23-f showed ADCC (46.7% cytotoxicity) against PC-10 cells more potently than did the control human IgG (14.6% cytotoxicity; P<0.01) (Figure 4B).

In the CDC of humLpMab-23-f against LN319 cells, humLpMab-23-f exhibited CDC (34.7% cytotoxicity) compared with that induced by control human IgG (11.6% cytotoxicity; P<0.05) (Figure 4C). Moreover, humLpMab-23-f exhibited CDC against PC-10 cells (53.4% cytotoxicity) compared with that induced by control human IgG (15.0% cytotoxicity; P<0.01) (Figure 4D).

These results demonstrated that humLpMab-23-f exhibited potent ADCC and CDC activities against endogenous PDPN-positive LN319 and PC-10 cells.

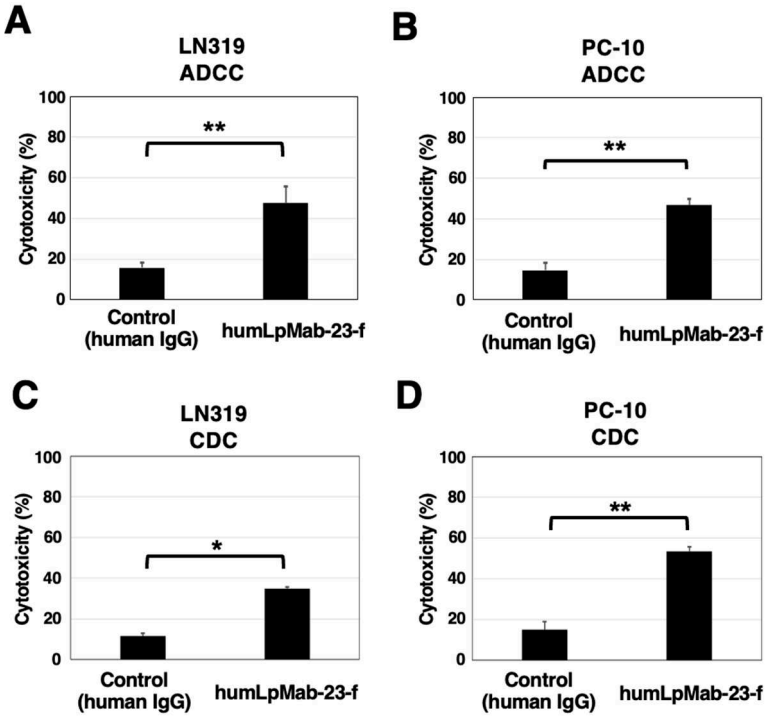

Figure 4. The ADCC and CDC activities mediated by humLpMab-23-f in PDPN-positive LN319 and PC-10 cells. (**A**,**B**) ADCC induced by humLpMab-23-f or control human IgG against LN319 (**A**) and PC-10 (**B**) cells. (**C**,**D**) CDC induced by humLpMab-23-f or control human IgG against LN319 (**C**) and PC-10 (**D**) cells. Values are shown as mean ± SEM. Asterisks indicate statistical significance (*P< 0.05, **P < 0.01; Welch's *t*-test). n.s., not significant. ADCC, antibody-dependent cellular cytotoxicity; CDC, complement-dependent cytotoxicity.

3.5. Antitumor effects of humLpMab-23-f in LN319 and PC-10 xenografts.

In the LN319 and PC-10 xenograft tumor-bearing mice, humLpMab-23-f and control human IgG were intraperitoneally injected on days 6, 14, and 21. Furthermore, human NK cells were injected around the tumors on days 6, 14, and 21. The tumor volume was measured on days 6, 11, 14, 18, 21, and 25 after the inoculation. The humLpMab-23-f administration resulted in a significant reduction in LN319 xenograft on days 21 (P<0.01) and 25 (P<0.01) compared with that of the control human IgG (Figure 5A). The humLpMab-23-f also showed a significant reduction in PC-10 xenograft on days 18 (P<0.01), 21 (P<0.01) and 25 (P<0.01) compared with that of the control human IgG (Figure 5B). The humLpMab-23-f administration resulted in a 64% (LN319) and a 69% (PC-10) reduction of tumor weight compared with that of the control human IgG on day 25 (Figure 5C,D). Tumors that were resected on day 25 are shown in Figure 5E,F.

The body weight loss was not observed in either LN319 or PC-10 xenograft-bearing mice treated with humLpMab-23-f and control human IgG (Figure 5G,H). Supplementary Figure S2 showed the

Preprints (www.preprints.org) | NOT PEER-REVIEWED | Posted: 24 August 2023 doi:10.20944/preprints202308.1756.v1

body appearance in LN319 and PC-10 xenografts-inoculated mice treated with human IgG and humLpMab-23-f on day 25.

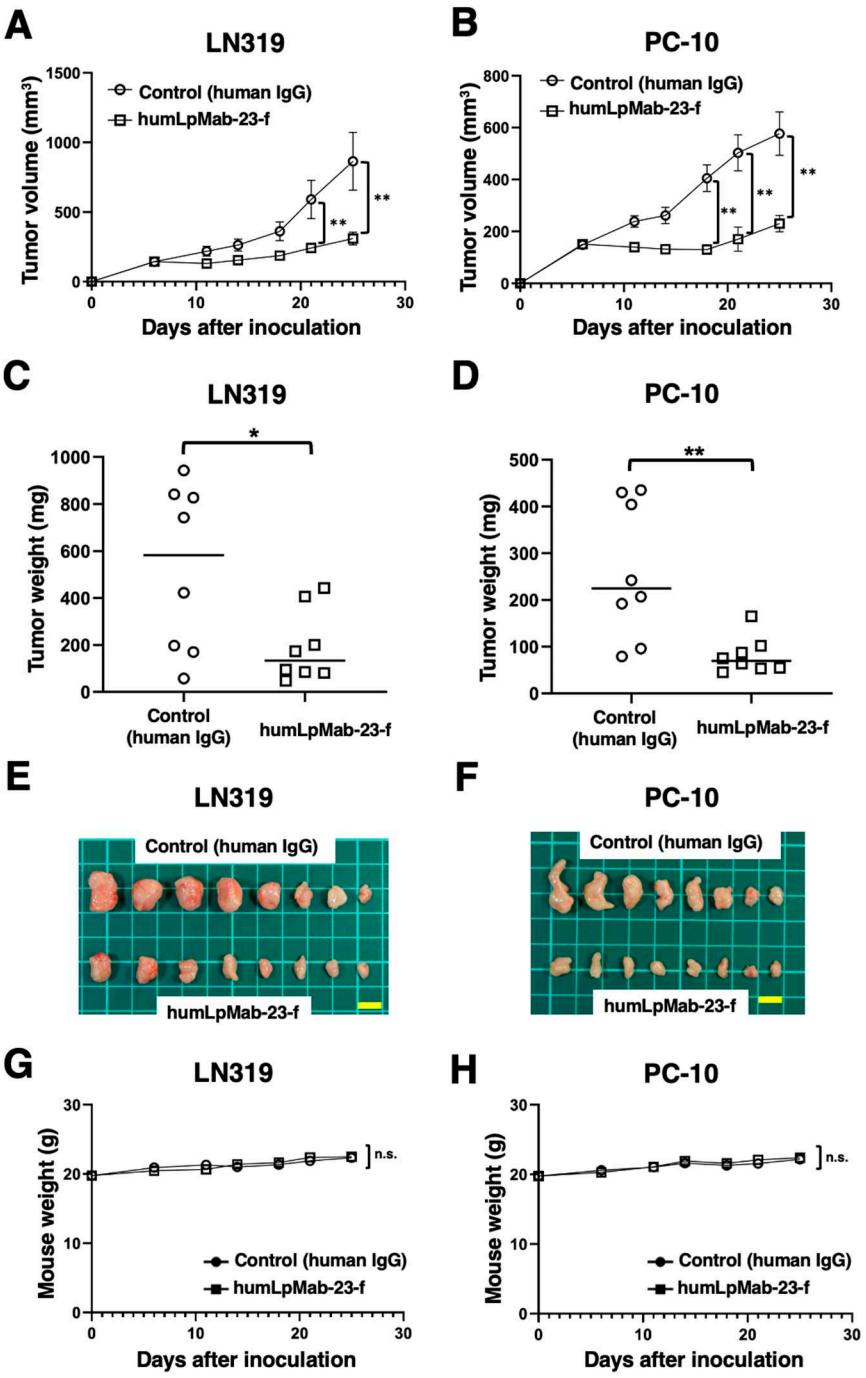

Figure 5. Antitumor activity of humLpMab-23-f against LN319 and PC-10 xenografts. (**A,B**) LN319 (**A**) and PC-10 (**B**) cells were subcutaneously injected into BALB/c nude mice (day 0). On day 6, 100 μg of humLpMab-23-f or control human IgG were intraperitoneally injected into mice. Additional antibodies were injected on days 14 and 21. The human NK cells were also injected around the tumors on days 6, 14, and 21. The tumor volume was measured on days 6, 11, 14, 18, 21, and 25. Values are presented as the mean ± SEM. **P <0.01 (ANOVA and Sidak's multiple comparisons test). (**C,D**) Tumor weight of LN319 (**C**) and PC-10 (**D**) xenograft tumors on day 25. Values are presented as the mean ± SEM. **P <0.01 (Welch's *t*-test). (**E, F**) The LN319 (**E**) and PC-10 (**F**) xenograft tumors on day 25 (scale bar, 1 cm). (**G,H**) The body weight of LN319 (**G**) and PC-10 (**H**) xenograft-bearing mice treated with control human IgG and humLpMab-23-f. n.s., not significant.

 doi:10.20944/preprints202308.1756.v1

4. Discussion

In this study, we showed that humLpMab-23-f exhibited potent ADCC and CDC activities against CHO/PDPN, PC-10, and LN319 cells (Figure 2 and Figure 4). Furthermore, administration of humLpMab-23-f in tumors-bearing mice completely suppressed the growth of CHO/PDPN xenograft (Figure 3A, C, and E) and exerted potent antitumor effects in PC-10 and LN319 xenografts (Figure 5). These results indicated that humLpMab-23-f could be useful for an antibody therapy for PDPN-positive human tumors.

We previously evaluated defucosylated mouse-human chimeric LpMab-23 (chLpMab-23-f) [27]. Although chLpMab-23-f exhibited ADCC activity and moderate antitumor effect against CHO/PDPN, chLpMab-23-f neither exhibited ADCC activity against PC-10 cells nor CDC against PDPN-expressing tumor cells [27]. The results of binding affinity revealed that K_D of humLpMab-23 against PC-10 was 5.4×10^{-9} M (Figure 1D). In contrast, K_D of chLpMab-23 against PC-10 was 1.4×10^{-7} M (Supplemental Figure S3). These results indicated that humLpMab-23 shows a superior binding affinity compared to chLpMab-23. The increased binding affinity is thought to be a reason why humLpMab-23-f exerted more potent antitumor effects than chLpMab-23.

PDPN is involved in the tumor malignant progression through activation of tumor invasiveness, EMT, and stemness. Furthermore, PDPN induces platelet aggregation through interaction with CLEC-2 on platelet, which is associated with venous thromboembolism and evasion of immune cells [37,38]. Therefore, several anti-PDPN mAbs have been evaluated in preclinical studies. Our group demonstrated that NZ-8 (a rat-human chimeric antibody derived from NZ-1) and chLpMab-7 (a mouse-human chimeric anti-PDPN mAb) showed antitumor effects through ADCC and CDC activities. Furthermore, NZ-1-R700 conjugate [39] and NZ-16 labeled with Actinium-225 (^{225}Ac) [40] have been developed as a near-infrared photoimmunotherapy and radioimmunotherapy against PDPN, respectively. Both mAbs also exhibited the antitumor effect against the malignant pleural mesothelioma xenograft model. In addition, the neutralizing mAbs for PDPN-CLEC-2 interaction also suppress hematogenous pulmonary metastasis by inhibiting platelet aggregation [41-43]. LpMab-23 has a different epitope from the abovementioned anti-PDPN mAbs [27], and showed comparable ADCC/CDC activities and antitumor effect *in vivo* (Figure 2-5). In contrast, the reactivity of LpMab-23 to normal cells such as lymphatic endothelial cells was low in immunohistochemical analysis [36]. It should be determined whether humLpMab-23-f possesses reduced cytotoxicity against normal PDPN-expressed cells.

CAFs are important players in the TME. CAFs involve in tumor progression through the promotion of tumor proliferation, invasion, chemoresistance as well as ECM remodeling and immunosuppression [44]. PDPN expression is also observed in CAFs. Increased expression of PDPN in CAFs from lung [19-21], breast [22], and pancreatic [23] is correlated with poor prognosis of patients. In PDPN-positive CAFs from lung tumors, the CAFs promote lung cancer cell resistance to inhibitors of EGFR [45]. Furthermore, increased expression of TGF-β was observed in PDPN-positive CAFs [21], which are associated with an immunosuppressive tumor microenvironment [18]. In breast cancer, the ratio S100A4/PDPN expression in the CAFs is associated with disease outcomes across subtypes. The high PDPN levels in the CAFs significantly correlated with shorter recurrence-free survival and overall survival [46]. Moreover, PDPN-positive CAFs was associated with low IL-2 activity and resistance to trastuzumab in HER2-positive breast cancer patients [47]. These findings indicate that the character of CAFs is an important predictive marker of breast cancer progression and resistance to treatment. Therefore, the targeting of PDPN-positive CAFs using anti-PDPN mAbs could be a strategy for tumor therapy.

The co-inhibitory receptors including PD-1 and CTLA-4 on effector T lymphocytes play a key role in tumor immunity. PDPN was reported as a co-inhibitory receptor on both $CD4^+$ and $CD8^+$ T lymphocytes. In T lymphocyte-specific *pdpn*-deleted mice, the growth of inoculated B16F10 tumor was significantly delayed. The pdpn-deficient $CD8^+$ tumor-infiltrating lymphocytes exhibited increased TNF production, and the exhausted T lymphocytes were decreased [48]. Moreover, a T cell-specific deletion of *pdpn* in mice spontaneously developed exacerbated autoimmune encephalomyelitis with increased accumulation of effector $CD4^+$ T lymphocytes [49]. These results

suggest the involvement of PDPN in tumor immune suppression. Although the ligand of PDPN to suppress T lymphocytes has not been identified, a PDPN-targeting mAb has potential as novel immune checkpoint inhibitor. We have established anti-PDPN mAbs against various species including mouse [1]. The anti-mouse PDPN mAb could be useful to reveal the importance of PDPN-positive lymphocytes in cancer immunity.

Author Contributions: H.S. and T.O. performed the experiments. M.K.K. and Y.K. designed the experiments. H.S. and Y.K. analyzed the data. H.S. and Y.K. wrote the manuscript. All authors have read and agreed to the manuscript.

Funding: This research was supported in part by Japan Agency for Medical Research and Development (AMED) under Grant Numbers: JP22ama121008 (to Y.K.), JP22am0401013 (to Y.K.), 23bm1123027h0001 (to Y.K.), JP22ck0106730 (to Y.K.), and JP21am0101078 (to Y.K.), and by the Japan Society for the Promotion of Science (JSPS) Grants-in-Aid for Scientific Research (KAKENHI) grant nos. 22K06995 (to H.S.), 21K07168 (to M.K.K.), and 22K07224 (to Y.K.).

Institutional Review Board Statement: Animal experiments were approved by the Institutional Committee for Experiments of the Institute of Microbial Chemistry (approval no. 2020-035).

Informed Consent Statement: Not applicable.

Data Availability Statement: The data presented in this study are available in the article and supplementary material.

Acknowledgments: The authors would like to thank Shun-ichi Ohba and Akiko Harakawa (Institute of Microbial Chemistry [BIKAKEN], Numazu, the Microbial Chemistry Research Foundation) for technical assistance with animal experiments.

Conflicts of Interest: The authors have no conflicts of interest to declare.

References

1. Suzuki, H.; Kaneko, M.K.; Kato, Y. Roles of Podoplanin in Malignant Progression of Tumor. *Cells* **2022**, *11*, doi:10.3390/cells11030575.
2. Kaneko, M.; Kato, Y.; Kunita, A.; Fujita, N.; Tsuruo, T.; Osawa, M. Functional sialylated O-glycan to platelet aggregation on Aggrus (T1alpha/Podoplanin) molecules expressed in Chinese hamster ovary cells. *J Biol Chem* **2004**, *279*, 38838-38843, doi:10.1074/jbc.M407210200.
3. Kaneko, M.K.; Kato, Y.; Kameyama, A.; Ito, H.; Kuno, A.; Hirabayashi, J.; Kubota, T.; Amano, K.; Chiba, Y.; Hasegawa, Y.; et al. Functional glycosylation of human podoplanin: glycan structure of platelet aggregation-inducing factor. *FEBS Lett* **2007**, *581*, 331-336, doi:10.1016/j.febslet.2006.12.044.
4. Sekiguchi, T.; Takemoto, A.; Takagi, S.; Takatori, K.; Sato, S.; Takami, M.; Fujita, N. Targeting a novel domain in podoplanin for inhibiting platelet-mediated tumor metastasis. *Oncotarget* **2016**, *7*, 3934-3946, doi:10.18632/oncotarget.6598.
5. Krishnan, H.; Rayes, J.; Miyashita, T.; Ishii, G.; Retzbach, E.P.; Sheehan, S.A.; Takemoto, A.; Chang, Y.W.; Yoneda, K.; Asai, J.; et al. Podoplanin: An emerging cancer biomarker and therapeutic target. *Cancer Sci* **2018**, *109*, 1292-1299, doi:10.1111/cas.13580.
6. Retzbach, E.P.; Sheehan, S.A.; Nevel, E.M.; Batra, A.; Phi, T.; Nguyen, A.T.P.; Kato, Y.; Baredes, S.; Fatahzadeh, M.; Shienbaum, A.J.; et al. Podoplanin emerges as a functionally relevant oral cancer biomarker and therapeutic target. *Oral Oncol* **2018**, *78*, 126-136, doi:10.1016/j.oraloncology.2018.01.011.
7. Li, Y.Y.; Zhou, C.X.; Gao, Y. Podoplanin promotes the invasion of oral squamous cell carcinoma in coordination with MT1-MMP and Rho GTPases. *Am J Cancer Res* **2015**, *5*, 514-529.
8. Zhao, P.; Xu, Y.; Wei, Y.; Qiu, Q.; Chew, T.L.; Kang, Y.; Cheng, C. The CD44s splice isoform is a central mediator for invadopodia activity. *J Cell Sci* **2016**, *129*, 1355-1365, doi:10.1242/jcs.171959.
9. Grass, G.D.; Tolliver, L.B.; Bratoeva, M.; Toole, B.P. CD147, CD44, and the epidermal growth factor receptor (EGFR) signaling pathway cooperate to regulate breast epithelial cell invasiveness. *J Biol Chem* **2013**, *288*, 26089-26104, doi:10.1074/jbc.M113.497685.
10. Wicki, A.; Lehembre, F.; Wick, N.; Hantusch, B.; Kerjaschki, D.; Christofori, G. Tumor invasion in the absence of epithelial-mesenchymal transition: podoplanin-mediated remodeling of the actin cytoskeleton. *Cancer Cell* **2006**, *9*, 261-272, doi:10.1016/j.ccr.2006.03.010.
11. de Winde, C.M.; George, S.L.; Crosas-Molist, E.; Hari-Gupta, Y.; Arp, A.B.; Benjamin, A.C.; Millward, L.J.; Makris, S.; Carver, A.; Imperatore, V.; et al. Podoplanin drives dedifferentiation and amoeboid invasion of melanoma. *iScience* **2021**, *24*, 102976, doi:10.1016/j.isci.2021.102976.

12. Kim, H.Y.; Rha, K.S.; Shim, G.A.; Kim, J.H.; Kim, J.M.; Huang, S.M.; Koo, B.S. Podoplanin is involved in the prognosis of head and neck squamous cell carcinoma through interaction with VEGF-C. *Oncol Rep* **2015**, *34*, 833-842, doi:10.3892/or.2015.4070.
13. Kreppel, M.; Drebber, U.; Wedemeyer, I.; Eich, H.T.; Backhaus, T.; Zöller, J.E.; Scheer, M. Podoplanin expression predicts prognosis in patients with oral squamous cell carcinoma treated with neoadjuvant radiochemotherapy. *Oral Oncol* **2011**, *47*, 873-878, doi:10.1016/j.oraloncology.2011.06.508.
14. Nakashima, Y.; Yoshinaga, K.; Kitao, H.; Ando, K.; Kimura, Y.; Saeki, H.; Oki, E.; Morita, M.; Kakeji, Y.; Hirahashi, M.; et al. Podoplanin is expressed at the invasive front of esophageal squamous cell carcinomas and is involved in collective cell invasion. *Cancer Sci* **2013**, *104*, 1718-1725, doi:10.1111/cas.12286.
15. Mishima, K.; Kato, Y.; Kaneko, M.K.; Nakazawa, Y.; Kunita, A.; Fujita, N.; Tsuruo, T.; Nishikawa, R.; Hirose, T.; Matsutani, M. Podoplanin expression in primary central nervous system germ cell tumors: a useful histological marker for the diagnosis of germinoma. *Acta Neuropathol* **2006**, *111*, 563-568, doi:10.1007/s00401-006-0033-4.
16. Mishima, K.; Kato, Y.; Kaneko, M.K.; Nishikawa, R.; Hirose, T.; Matsutani, M. Increased expression of podoplanin in malignant astrocytic tumors as a novel molecular marker of malignant progression. *Acta Neuropathol* **2006**, *111*, 483-488, doi:10.1007/s00401-006-0063-y.
17. Abe, S.; Morita, Y.; Kaneko, M.K.; Hanibuchi, M.; Tsujimoto, Y.; Goto, H.; Kakiuchi, S.; Aono, Y.; Huang, J.; Sato, S.; et al. A novel targeting therapy of malignant mesothelioma using anti-podoplanin antibody. *J Immunol* **2013**, *190*, 6239-6249, doi:10.4049/jimmunol.1300448.
18. Sakai, T.; Aokage, K.; Neri, S.; Nakamura, H.; Nomura, S.; Tane, K.; Miyoshi, T.; Sugano, M.; Kojima, M.; Fujii, S.; et al. Link between tumor-promoting fibrous microenvironment and an immunosuppressive microenvironment in stage I lung adenocarcinoma. *Lung Cancer* **2018**, *126*, 64-71, doi:10.1016/j.lungcan.2018.10.021.
19. Hoshino, A.; Ishii, G.; Ito, T.; Aoyagi, K.; Ohtaki, Y.; Nagai, K.; Sasaki, H.; Ochiai, A. Podoplanin-positive fibroblasts enhance lung adenocarcinoma tumor formation: podoplanin in fibroblast functions for tumor progression. *Cancer Res* **2011**, *71*, 4769-4779, doi:10.1158/0008-5472.Can-10-3228.
20. Sasaki, K.; Sugai, T.; Ishida, K.; Osakabe, M.; Amano, H.; Kimura, H.; Sakuraba, M.; Kashiwa, K.; Kobayashi, S. Analysis of cancer-associated fibroblasts and the epithelial-mesenchymal transition in cutaneous basal cell carcinoma, squamous cell carcinoma, and malignant melanoma. *Hum Pathol* **2018**, *79*, 1-8, doi:10.1016/j.humpath.2018.03.006.
21. Suzuki, J.; Aokage, K.; Neri, S.; Sakai, T.; Hashimoto, H.; Su, Y.; Yamazaki, S.; Nakamura, H.; Tane, K.; Miyoshi, T.; et al. Relationship between podoplanin-expressing cancer-associated fibroblasts and the immune microenvironment of early lung squamous cell carcinoma. *Lung Cancer* **2021**, *153*, 1-10, doi:10.1016/j.lungcan.2020.12.020.
22. Pula, B.; Jethon, A.; Piotrowska, A.; Gomulkiewicz, A.; Owczarek, T.; Calik, J.; Wojnar, A.; Witkiewicz, W.; Rys, J.; Ugorski, M.; et al. Podoplanin expression by cancer-associated fibroblasts predicts poor outcome in invasive ductal breast carcinoma. *Histopathology* **2011**, *59*, 1249-1260, doi:10.1111/j.1365-2559.2011.04060.x.
23. Shindo, K.; Aishima, S.; Ohuchida, K.; Fujiwara, K.; Fujino, M.; Mizuuchi, Y.; Hattori, M.; Mizumoto, K.; Tanaka, M.; Oda, Y. Podoplanin expression in cancer-associated fibroblasts enhances tumor progression of invasive ductal carcinoma of the pancreas. *Mol Cancer* **2013**, *12*, 168, doi:10.1186/1476-4598-12-168.
24. Mir Seyed Nazari, P.; Riedl, J.; Pabinger, I.; Ay, C. The role of podoplanin in cancer-associated thrombosis. *Thromb Res* **2018**, *164 Suppl 1*, S34-s39, doi:10.1016/j.thromres.2018.01.020.
25. Kato, Y.; Kunita, A.; Abe, S.; Ogasawara, S.; Fujii, Y.; Oki, H.; Fukayama, M.; Nishioka, Y.; Kaneko, M.K. The chimeric antibody chLpMab-7 targeting human podoplanin suppresses pulmonary metastasis via ADCC and CDC rather than via its neutralizing activity. *Oncotarget* **2015**, *6*, 36003-36018, doi:10.18632/oncotarget.5339.
26. Kato, Y.; Kaneko, M.K. A cancer-specific monoclonal antibody recognizes the aberrantly glycosylated podoplanin. *Sci Rep* **2014**, *4*, 5924, doi:10.1038/srep05924.
27. Kaneko, M.K.; Nakamura, T.; Kunita, A.; Fukayama, M.; Abe, S.; Nishioka, Y.; Yamada, S.; Yanaka, M.; Saidoh, N.; Yoshida, K.; et al. ChLpMab-23: Cancer-Specific Human-Mouse Chimeric Anti-Podoplanin Antibody Exhibits Antitumor Activity via Antibody-Dependent Cellular Cytotoxicity. *Monoclon Antib Immunodiagn Immunother* **2017**, *36*, 104-112, doi:10.1089/mab.2017.0014.
28. Kaneko, M.K.; Yamada, S.; Nakamura, T.; Abe, S.; Nishioka, Y.; Kunita, A.; Fukayama, M.; Fujii, Y.; Ogasawara, S.; Kato, Y. Antitumor activity of chLpMab-2, a human-mouse chimeric cancer-specific antihuman podoplanin antibody, via antibody-dependent cellular cytotoxicity. *Cancer Med* **2017**, *6*, 768-777, doi:10.1002/cam4.1049.
29. Ishikawa, A.; Waseda, M.; Ishii, T.; Kaneko, M.K.; Kato, Y.; Kaneko, S. Improved anti-solid tumor response by humanized anti-podoplanin chimeric antigen receptor transduced human cytotoxic T cells in an animal model. *Genes Cells* **2022**, *27*, 549-558, doi:10.1111/gtc.12972.
30. Chalise, L.; Kato, A.; Ohno, M.; Maeda, S.; Yamamichi, A.; Kuramitsu, S.; Shiina, S.; Takahashi, H.; Ozone, S.; Yamaguchi, J.; et al. Efficacy of cancer-specific anti-podoplanin CAR-T cells and oncolytic herpes virus

G47Δ combination therapy against glioblastoma. *Mol Ther Oncolytics* **2022**, *26*, 265-274, doi:10.1016/j.omto.2022.07.006.

31. Shiina, S.; Ohno, M.; Ohka, F.; Kuramitsu, S.; Yamamichi, A.; Kato, A.; Motomura, K.; Tanahashi, K.; Yamamoto, T.; Watanabe, R.; et al. CAR T Cells Targeting Podoplanin Reduce Orthotopic Glioblastomas in Mouse Brains. *Cancer Immunol Res* **2016**, *4*, 259-268, doi:10.1158/2326-6066.CIR-15-0060.
32. Shinkawa, T.; Nakamura, K.; Yamane, N.; Shoji-Hosaka, E.; Kanda, Y.; Sakurada, M.; Uchida, K.; Anazawa, H.; Satoh, M.; Yamasaki, M.; et al. The absence of fucose but not the presence of galactose or bisecting N-acetylglucosamine of human IgG1 complex-type oligosaccharides shows the critical role of enhancing antibody-dependent cellular cytotoxicity. *J Biol Chem* **2003**, *278*, 3466-3473, doi:10.1074/jbc.M210665200.
33. Yamane-Ohnuki, N.; Kinoshita, S.; Inoue-Urakubo, M.; Kusunoki, M.; Iida, S.; Nakano, R.; Wakitani, M.; Niwa, R.; Sakurada, M.; Uchida, K.; et al. Establishment of FUT8 knockout Chinese hamster ovary cells: an ideal host cell line for producing completely defucosylated antibodies with enhanced antibody-dependent cellular cytotoxicity. *Biotechnol Bioeng* **2004**, *87*, 614-622, doi:10.1002/bit.20151.
34. Suzuki, H.; Ohishi, T.; Asano, T.; Tanaka, T.; Saito, M.; Mizuno, T.; Yoshikawa, T.; Kawada, M.; Kaneko, M.K.; Kato, Y. Defucosylated mouse-dog chimeric anti-HER2 monoclonal antibody exerts antitumor activities in mouse xenograft models of canine tumors. *Oncol Rep* **2022**, *48*, doi:10.3892/or.2022.8366.
35. Yamada, S.; Ogasawara, S.; Kaneko, M.K.; Kato, Y. LpMab-23: A Cancer-Specific Monoclonal Antibody Against Human Podoplanin. *Monoclon Antib Immunodiagn Immunother* **2017**, *36*, 72-76, doi:10.1089/mab.2017.0001.
36. Miyazaki, A.; Nakai, H.; Sonoda, T.; Hirohashi, Y.; Kaneko, M.K.; Kato, Y.; Sawa, Y.; Hiratsuka, H. LpMab-23-recognizing cancer-type podoplanin is a novel predictor for a poor prognosis of early stage tongue cancer. *Oncotarget* **2018**, *9*, 21156-21165, doi:10.18632/oncotarget.24986.
37. Takemoto, A.; Miyata, K.; Fujita, N. Platelet-activating factor podoplanin: from discovery to drug development. *Cancer Metastasis Rev* **2017**, *36*, 225-234, doi:10.1007/s10555-017-9672-2.
38. Fujita, N.; Takagi, S. The impact of Aggrus/podoplanin on platelet aggregation and tumour metastasis. *J Biochem* **2012**, *152*, 407-413, doi:10.1093/jb/mvs108.
39. Nishinaga, Y.; Sato, K.; Yasui, H.; Taki, S.; Takahashi, K.; Shimizu, M.; Endo, R.; Koike, C.; Kuramoto, N.; Nakamura, S.; et al. Targeted Phototherapy for Malignant Pleural Mesothelioma: Near-Infrared Photoimmunotherapy Targeting Podoplanin. *Cells* **2020**, *9*, doi:10.3390/cells9041019.
40. Sudo, H.; Tsuji, A.B.; Sugyo, A.; Kaneko, M.K.; Kato, Y.; Nagatsu, K.; Suzuki, H.; Higashi, T. Preclinical Evaluation of Podoplanin-Targeted Alpha-Radioimmunotherapy with the Novel Antibody NZ-16 for Malignant Mesothelioma. *Cells* **2021**, *10*, doi:10.3390/cells10102503.
41. Kato, Y.; Kaneko, M.K.; Kunita, A.; Ito, H.; Kameyama, A.; Ogasawara, S.; Matsuura, N.; Hasegawa, Y.; Suzuki-Inoue, K.; Inoue, O.; et al. Molecular analysis of the pathophysiological binding of the platelet aggregation-inducing factor podoplanin to the C-type lectin-like receptor CLEC-2. *Cancer Sci* **2008**, *99*, 54-61, doi:10.1111/j.1349-7006.2007.00634.x.
42. Kato, Y.; Kaneko, M.K.; Kuno, A.; Uchiyama, N.; Amano, K.; Chiba, Y.; Hasegawa, Y.; Hirabayashi, J.; Narimatsu, H.; Mishima, K.; et al. Inhibition of tumor cell-induced platelet aggregation using a novel anti-podoplanin antibody reacting with its platelet-aggregation-stimulating domain. *Biochem Biophys Res Commun* **2006**, *349*, 1301-1307, doi:10.1016/j.bbrc.2006.08.171.
43. Ukaji, T.; Takemoto, A.; Katayama, R.; Takeuchi, K.; Fujita, N. A safety study of newly generated anti-podoplanin-neutralizing antibody in cynomolgus monkey (Macaca fascicularis). *Oncotarget* **2018**, *9*, 33322-33336, doi:10.18632/oncotarget.26055.
44. Gascard, P.; Tlsty, T.D. Carcinoma-associated fibroblasts: orchestrating the composition of malignancy. *Genes Dev* **2016**, *30*, 1002-1019, doi:10.1101/gad.279737.116.
45. Yoshida, T.; Ishii, G.; Goto, K.; Neri, S.; Hashimoto, H.; Yoh, K.; Niho, S.; Umemura, S.; Matsumoto, S.; Ohmatsu, H.; et al. Podoplanin-positive cancer-associated fibroblasts in the tumor microenvironment induce primary resistance to EGFR-TKIs in lung adenocarcinoma with EGFR mutation. *Clin Cancer Res* **2015**, *21*, 642-651, doi:10.1158/1078-0432.Ccr-14-0846.
46. Friedman, G.; Levi-Galibov, O.; David, E.; Bornstein, C.; Giladi, A.; Dadiani, M.; Mayo, A.; Halperin, C.; Pevsner-Fischer, M.; Lavon, H.; et al. Cancer-associated fibroblast compositions change with breast cancer progression linking the ratio of S100A4(+) and PDPN(+) CAFs to clinical outcome. *Nat Cancer* **2020**, *1*, 692-708, doi:10.1038/s43018-020-0082-y.
47. Rivas, E.I.; Linares, J.; Zwick, M.; Gómez-Llonin, A.; Guiu, M.; Labernadie, A.; Badia-Ramentol, J.; Lladó, A.; Bardia, L.; Pérez-Núñez, I.; et al. Targeted immunotherapy against distinct cancer-associated fibroblasts overcomes treatment resistance in refractory HER2+ breast tumors. *Nat Commun* **2022**, *13*, 5310, doi:10.1038/s41467-022-32782-3.
48. Chihara, N.; Madi, A.; Kondo, T.; Zhang, H.; Acharya, N.; Singer, M.; Nyman, J.; Marjanovic, N.D.; Kowalczyk, M.S.; Wang, C.; et al. Induction and transcriptional regulation of the co-inhibitory gene module in T cells. *Nature* **2018**, *558*, 454-459, doi:10.1038/s41586-018-0206-z.

49. Peters, A.; Burkett, P.R.; Sobel, R.A.; Buckley, C.D.; Watson, S.P.; Bettelli, E.; Kuchroo, V.K. Podoplanin negatively regulates CD4+ effector T cell responses. *J Clin Invest* **2015**, *125*, 129-140, doi:10.1172/jci74685.